JOURNAL OF MATERIALS SCIENCE **38** (2003) 1219–1229

Effect of the addition of Ca^{2+} on the structure, microstructure and ferroelectric properties of $(Pb_{1-y}Ca_y)(Zr_{0.8}Ti_{0.2})O_3$ system with $y = 0.0$, 0.02, 0.05 and 0.1

ALI BEITOLLAHI
Department of Metallurgy & Materials Engineering, Iran University of Science & Technology, Narmak, Tehran, Iran
E-mail: beitolla@iust.ac.ir

This work studies the relationship between ferroelectric properties and structural features of the $(Pb_{1-y}Ca_y)(Zr_{0.8}Ti_{0.2})O_3$ system with $y = 0.0$, 0.02, 0.05 and 0.1. All of the samples were prepared by hot-pressing of PZT calcined powder, prepared by conventional ceramic route. Single phase compositions of rhombohedral (RH) structure were observed for the whole series of the samples studied in this work. However, a linear decrease of RH lattice constant a_p is seen with increasing the Ca^{2+} concentration with a subsequent decrease of lattice strain expressed by $(90 - \alpha_p)$. Further, a sharp decline is also observed in the magnitudes of saturation polarization (P_s) of the samples doped with 2 mol% Ca^{2+}. However, the rate of decrease slows down for Ca^{2+} concentrations above this level. A diffuse phase transition was observed in the case of 10 mol% Ca^{2+}-doped PZT(0.8) which is believed to be possibly due to the distribution in coupling strengths created from a random compositional fluctuations of Ca^{2+} and Pb^{2-} ions on A-sites. The results are interpreted on crystal-chemical grounds. It is proposed that the long range coupling of $(Zr/Ti)O_6$ coordination octahedra and Pb^{2+} ions, due to the covalency of the Pb–O bond, is interrupted by the incorporation of Ca^{2+}. By considering the effect of calcium on coupling strength and coupling distribution, the observed dielectric response for the above compositions is qualitatively explained.

1. Introduction

Ferroelectric materials and related oxide ceramics find one of the widest range of applications amongst ceramic based components in the electronic industry, thereby ranking in importance second only to semiconductors. These applications include pyroelectric sensors for thermal detectors, dielectrics for capacitors, piezoelectric materials for electromechanical transducers, microwave resonators etc. Lead zirconate titanate, $PbZr_{1-x}Ti_xO_3$ (PZT), is known for its very interesting properties which is adapted with its various structural modifications and when it is doped with various dopants [1]. Fig. 1 displays the ferroelectric phase diagram of this compound. There are two interesting regions in this phase diagram. One belongs to the PZ-rich regions which shows interesting properties for thermal detector applications, because of the low permittivities and high pyroelectric coefficients seen for the compounds of this region [2]. The second one, is that of morphotropic region corresponding to Zr/Ti = 53/47 which is known as the best compositional region for piezoelectric applications. New features of MPB region have also been recently reported. A new monoclinic ferroelectric phase was discovered at low temperatures and various properties of which were studied using techniques such as high resolution synchrotron X-ray powder diffraction, Raman spectroscopy and dielectric measurements [3–5]. As this phase digram shows, $PbZrO_3$(PZ)-rich materials adopt rhombohedral symmetry with the polar axis lying along ⟨111⟩ directions and for the compositions comprising almost entirely $PbZrO_3$, orthorhombic symmetry is found with the polar axis along ⟨110⟩ directions; however, this phase is associated with antiferroelectric properties. For the compositions with $0.03 < x < 0.08$, Handerek *et al.* [6, 7]. And Ujima *et al.* [8], based on XRD measurements have revealed the coexistence of the antiferroelectric phase (normally presented with A_O) and F_R(LT) phases. Further, Chang Y. I. [9] have also confirmed, using TEM technique, the coexistence of these phases for PZT compound of Zr/Ti = 95/5. In $PbTiO_3$-rich compositions a tetragonal structure in which the polar axis is aligned in ⟨001⟩ directions is seen. Further, P_c represents the cubic paraelectric phase, F_T, a ferroelectric tetragonal phase, and F_R(LT) and F_R(HT), the low and high temperature forms of a rhombohedral ferroelectric phase verified by neutron diffraction experiment [10] (Fig. 1). For F_R(LT) region, the Pb and Zr/Ti atoms are displaced parallel

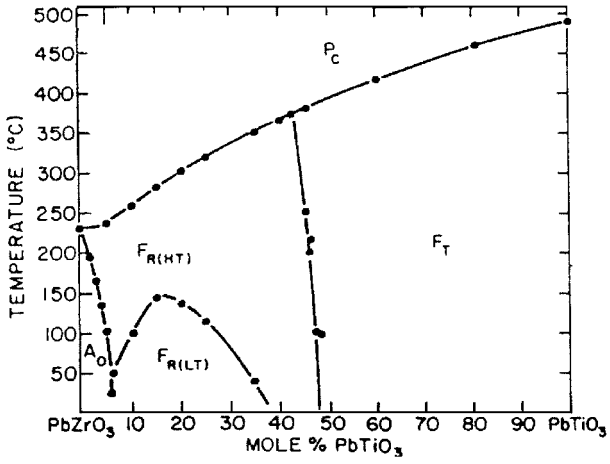

Figure 1 Phase diagram of the PZT system [1].

to one another along [111] to give a polar ferroelectric phase. In addition the oxygen octahedra are tilted about [111] to give rise to a doubled unit cell. In the notation of Glazer [11, 12], this is represented by the tilt system $a^- a^- a^-$ and results in cell doubling of all of three pseudo-cubic axes, hence forming a unti cell containing eight formula units. Doubling of the unit cell axes, due to the tilting of the octahedra, causes extra reflections which lie on half-integral reciprocal-lattice planes.

At higher temperatures (as high as 100°C) these tilts are lost in the F_R(HT) phase, but cation shifts are retained, thus preserving polarization. Finally at 250°C the cation displacements are also lost to form the paraelectric cubic phase. Therefore, for the compositions in the F_R(LT) region, there are two contributing sources for the saturation polarisation (P_s) one; Pb displacements along [111] and the second oxygen octahedra tilt along [111]. On moving from F_R(LT) phase to F_R (HT) phase the tilt is lost and the Pb displacements will be the only source of polarization before reaching cubic paraelectric phase.

Substituting Ba^{2+} for Pb^{2+} in PZT, is seen [13] to decrease the RH lattice distortion. The magnitude of the decline also increases as the Ba^{2-} content increases. Ikeda [14] has shown that doping PZ-rich PZT compositions with Sr^{2+} causes the formation of an antiferroelectric phase of tetragonal structure at room temperature. Further, the field of stability of this phase increases by increasing Sr^{2+} concentration. However, doping PZ-rich PZT compositions with Ba^{2+} suppresses completely the antiferroelectric orthorhombic phase observed originally in case of undoped PZT [13]. It is shown that doping PZT(0.9)(Zr/Ti = 9) [13] or pure $PbZrO_3$ [15] with 20 mol% Ba^{2+} promotes the formation of a ferroelectric RH phase. The stabilization of an specific ionic crystal structure is related to the chemical nature of the ions involved, their size, their degrees of ionicity and also their respective electronegativities. Based on these works, one can find that, whilst addition of Ba^{2+} to PZ-rich PZT compositions suppresses the formation of antiferroelectric phase, Sr^{2+} and Ca^{2+} promote its formation. The author, in a systematic work have tried to interpret the effect of the addition of Ca^{2+} on the structural, and ferroelectric properties of PZ-rich PZT compounds in the form of; $(Pb_{1-y}Ca_y)(Zr_{1-x}Ti_x)O_3$ with $y = 0.0$, 0.02, 0.05 and 0.1 and $x = 0.1$, 0.15 and 0.2, based on a crystal—chemical approach. Here, the results of the first series, i.e. $x = 0.2$, and $y = 0.0$, 0.02, 0.05 and 0.1 are presented.

2. Experimentals

The composition chosen to be studied was: $PbZr_{0.8}Ti_{0.2}O_3$ doped separately with 2, 5 and 10 mol% CaO, according to the formula; $Pb_{1-y}Ca_yZr_{1-x}Ti_xO_3$ with ($y = 0.0$, 0.02, 0.05 and 0.1) and ($x = 0.2$). Conventional ceramic preparation routes were employed to prepare PZT powders in this work. These were later hot-pressed to prepare high density samples. The purity of PbO and TiO_2 powders obtained from Aldrich was better than 99.9%. ZrO_2 powder initially used for PZT sample preparation was obtained from Tosoh–Zirconia TZ-0 (99.9%).

The specific surface area reported in the analysis document of ZrO_2 powder was 13 m^2/g. The appropriate amounts of the starting powders were weighed by an electronic balance with an accuracy of 0.1 mg, in accordance with the formula of the composition chosen. These were subsequently subjected to a mixing process in polypropylene bottles. The mixing media liquid was propan-2-ol and zirconia cylinders ($1/2'' \times 1/2''$) were also used to initiate the mixing and milling process. Each composition was milled for 8 hrs. These were then dried under a U.V. heat lamp. The dried milled powders were then sieved through a 100 μm polyester sieve. The sieved powders of each composition were calcined in a closed pure Al_2O_3 crucible at 4 different temperatures (750, 800, 850, and 900°C) for a fixed soaking time of 2 hrs. Refractory cement was used to attach the lid to the outer wall of crucible, thereby reducing the loss of PbO from the calcination environment. The calcined powder was then subjected to a wet milling process (media liquid propan-2-ol) for 16 hrs with zirconia cylinders ($1/2'' \times 1/2''$) as milling agents. X-ray diffraction (Cu $K_{\alpha 1}$ radiation) was used to detect the phases formed during the calcination process. Single phase compounds of rhombohedral structure could only be formed when calcined at 900°C for 2 hrs. The measured lead loss at this temperature, which was determined from measurement of the pellet weight before and after calcination was, however, found to be quite high (~1%). Therefore, it was decided to use very fine ZrO_2 powder to promote the reactivity of the solid state reactions taking place during the calcination process. Ultrafine ZrO_2 powders were initially prepared by the alkoxide route the detail of which is explained elesevere [16]. The surface area of the powder prepared by the BET technique (Perkin Elmer Sorpometer 212D) was found to be 96 m^2/g. PZT powders, of compositions similar to those prepared with commercial ZrO_2 powder, were prepared by an identical preparation route but this time using chemically prepared ZrO_2 powder. However, X-ray analysis of the calcined product confirmed the formation of single phase rhombohedral structure at temperatures as low as 750°C.

Furthermore, the measured lead losses at this temperature were found to be negligible. It was therefore decided to use the chemically prepared ZrO_2 powder for the preparation of the whole series of calcium doped and undoped PZT compositions in this work. In addition, for the calcium doped compositions, it was decided to use a solution of calcium nitrate ($Ca(NO_3)_2$, 99.9%) in propan-2-ol. This permitted the introduction of calcium in solution, thereby giving a homogeneous distribution of calcium in the ceramic samples. Different calcined powders were prepared by this route, with each subsequently milled for 16 hrs with zirconia cylinders ($1/2'' \times 1/2''$). The particle size distribution was also determined using an X-ray sedimentometer. All samples were hot-pressed in oxygen, using equipment built 'in house' using an alumina die. Pellets were surrounded by a magnesium oxide grit (Mandoval Ltd., Surrey, UK) (100 μm particle size) to prevent contact between the alumina die component and the sample, and to allow the formation of a lead-rich reaction zone around the pellet during sintering. A uniaxial pressure could be applied to the die-punches, from above, using a hydraulic ram. The die-set was surrounded by an alumina cylinder into which oxygen gas was injected. The hot-pressing temperature for all of the samples studied was 1200°C, applied for 1 hour. For a comparative study, some samples were also prepared at 1300°C for 2 hrs. The applied pressure for all these cases was 10 MPa, with an oxygen flow-rate of 5 $cm^3\ min^{-1}$. Prior to characterization, the MgO-reacted layers were ground from the surface of the hot-pressed boules. Microstructural analysis of the whole series of samples was performed by scanning electron microscope (SEM). Fracture surface analysis was used to investigate the morphology of the grains as well as their size distribution. Before each examination by this technique, the specimens were sputter-coated with gold and examined in a Hitachi S-700 high resolution SEM. Fig 2a and b demonstrate the typical microstructure for an undoped $Pb(Zr_{0.8}Ti_{0.2})O_3$ composition and the same composition doped with 10 mol% calcium, both hot-pressed at 1200°C for 1 hr.

The increase in densities which follow from the decrease in porosities of the former compositions are observable in these micrographs. However, no appreciable grain growth was observed for any of Ca^{2+}-doped samples compared to undoped ones, during the examination of these samples. A typical grain size range of between 1 to 2 μm, in the case of undoped samples and 1.5 to 2.5 μm for doped samples was obtained from the flat polished and etched samples. Generally a very uniform grain size distribution could be observed for all of the samples and no abnormal grain growth was detected. The densities of all samples were measured using the water immersion method. Quantitative chemical analysis was done by electron probe microanalysis (EPMA) technique in which the concentration of an element is determined by the ratio of the number of counts of characteristic X-rays emitted in a fixed time from the specimen, relative to those emitted from a standard of known composition. Specimens before measurement were mounted and polished to 1/4 μm, prior to being

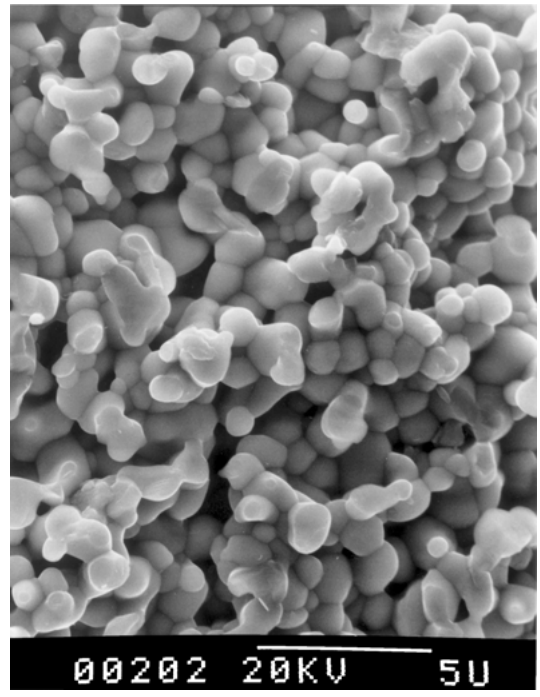

(a)

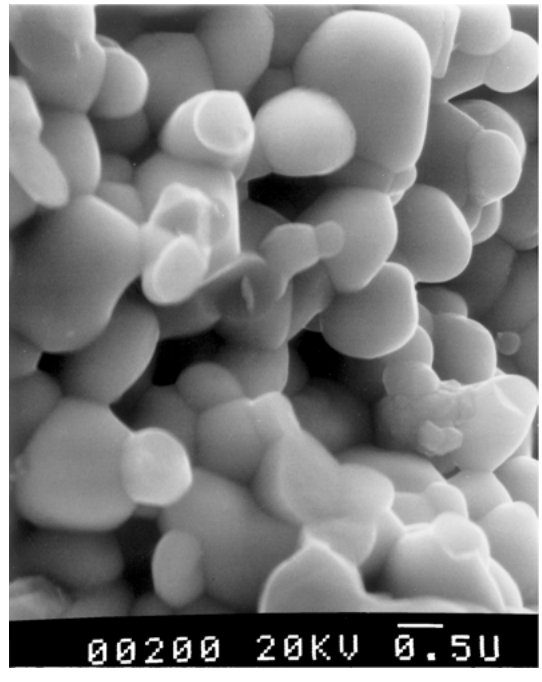

(b)

Figure 2 (a) SEM micrograph of $Pb(Zr_{0.8}Ti_{0.2})O_3$: hot-pressed at 1200°C for 1 h. (b) SEM micrograph of $Pb(Zr_{0.8}Ti_{0.2})O_3$ doped with 10 mol% Ca^{2+}; hot-pressed at 1200°C for 1 h.

coated with a thin layer of carbon. Analyses were made using a CAMECA SX50. The system was operated at 20 kV with a 1 nA beam current and a lifetime of 100 s. Analyses taken from the edges of specimens revealed that there were no significant deviations from the required compositions, suggesting that there was no lead depletion at the edges. Additional analyses, checking for the possible introduction of Zr^{4+}, as a possible impurity from the milling process, did not confirm its presence. It was, therefore, concluded that ceramic samples in the solid solution $(Pb_{1-y}Ca_y)(Zr_{0.8}Ti_{0.2})O_3$

system with $y = 0.0$, 0.02, 0.05 and 0.1 were fabricated with the required chemical compositions. Room temperature X-ray diffraction studies were carried out with a Philips APD 1700 automatic powder diffraction system, in conjunction with a Micro VAX-3100 computer. The diffractometer was operated at 40 kV with 20 mA current. Monochromatic Cu $K_{\alpha 1}$ radiation of wavelength 1. 54060 Å was used throughout. For all measurements, a scan step mode was used with a step size of 0.005° every 2 seconds. Each sample was scanned for a 2θ-range from 10–70°. Prior to each measurement, the samples were crushed and pulverised with a pestle and mortar. The obtained fine powders were then mixed with a pure silicon powder (99.9%) which was used as the standard sample, with a sample to silicon powder weight ratio of (2:1). A computer program, was used to determine lattice parameters of the samples. Flat and polished samples were coated with platinium to measure the dielectric properties and polarisations of the studied samples. Two different computer controlled set-up were used for permittivity and dielectric loss measurements in conjunction with two temperature controlled chambers each one capable of measuring relative permittivity and loss at a different temperature range. The first of these had a temperature range between −100 and 100°C, with the other operating between r.t. and 400°C. An 'in house' built computerised Sawyer-Tower circuit was used to measure the E-P variations of the samples studied at room temperature. The specimens used for this measurement were also prepared in an identical manner applied for dielectric measurements. The samples were loaded into a test-fixture surrounded with silicone oil to prevent surface leakage breakdown during application of high electric field. The maximum applied field was chosen to be sufficient to produce saturated polarization.

3. Results

3.1. X-ray diffraction

Fig. 3 presents a multiplot of r.t. X-ray diffraction patterns for the series of composition of formula: $(Pb_{1-y}Ca_y)(Zr_{0.8}Ti_{0.2})O_3$, where $y = 0.0$, 0.02, 0.05 and 0.1, using Cu $K_{\alpha 1}$ radiation for 2θ angles between 10° and 70°. For this series of compositions, no second phase was observed, within the limit of experimental accuracy. This suggests the formation of single phase solid solution, with Ca^{2+} in the A site. The similarity of the diffraction patterns (Fig. 3) also suggests the formation of a similar structure for all of the compounds of this series. Furthermore, as can be seen from this multiplot, reflections such as *hhh* are split while *h*00 are not. Thus it can be inferred that the structure is rhombohedral (RH). However, the observed rhombohedral splitting decreases on going from undoped PZT(0.8) towards the composition PZT(0.8) doped with 10 mol% Ca^{2+}, where it becomes very small (Fig. 3).

TABLE I Calculated values of lattice parameters for the PZT(0.8) series

Composition	a_p (Å)	E.S.D	α_p(°)	E.S.D
PZT(0.8)	4.1216	0.0007	89.697	0.002
PZT(0.8) doped with 2 mol% Ca.	4.1160	0.0004	89.768	0.0016
PZT(0.8) doped with 5 mol% Ca.	4.1092	0.0005	89.786	0.0012
PZT(0.8) doped with 10 mol% Ca.	4.0987	0.0005	89.861	0.0019

Table I presents the obtained values of lattice parameters with calculated E.S.D values, as well as the interaxial angle (α_p) for this series of compositions. Figs 4 and 5 show the variation of rhombohedral lattice constant (a_p) as well as interaxial angle (α_p) for this series of compositions at room temperature. As shown, a_p decreases linearly with Ca^{2+} concentration. The curve of the variation of RH lattice strain expressed by $(90° - \alpha_p)$ with Ca^{2+} concentration is also shown in Fig. 6. As this curve implies, the lattice strain decreases sharply by substituting Ca^{2+} for Pb^{+2} for this series of compositions. This is also in agreement with the observed reduction in the width of split reflections.

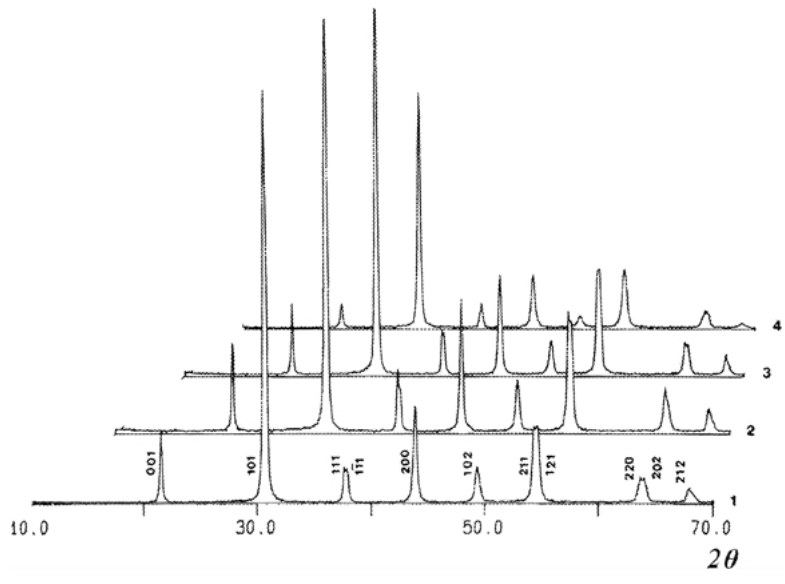

Figure 3 X-ray diffraction multiplot of $Pb_{1-y}Ca_y(Zr_{0.8}Ti_{0.2})O_3$ system with $y = 0.0(1)$, 0.02(2), 0.05(3), 0.1(4), hot-pressed at 1200°C for 1 hour.

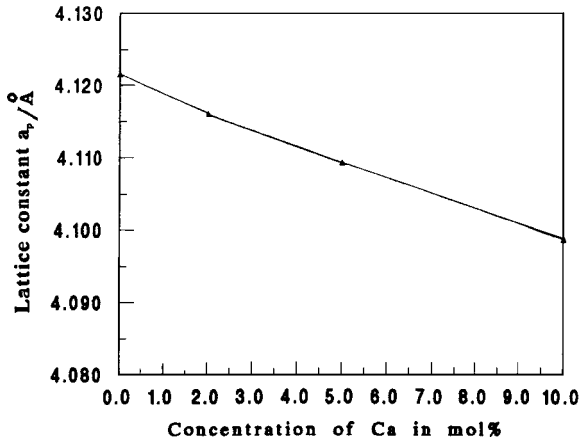

Figure 4 Room temperature lattice constant (a_p) as a function of Ca^{2+} content for $Pb_{1-y}Ca_y(Zr_{0.8}Ti_{0.2})O_3$ system.

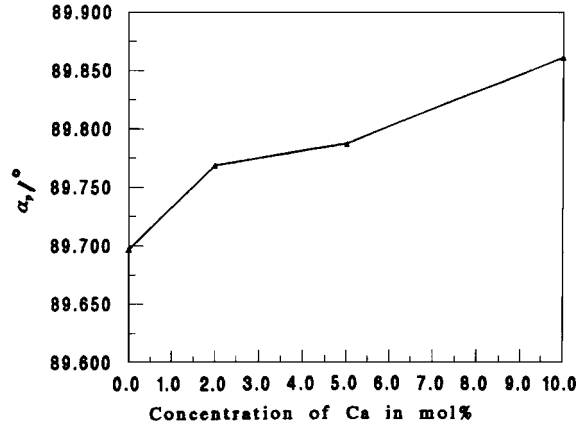

Figure 5 Rhombohedral interaxial angle as a function of Ca^{2+} content for $Pb_{1-y}Ca_y(Zr_{0.8}Ti_{0.2})O_3$ system.

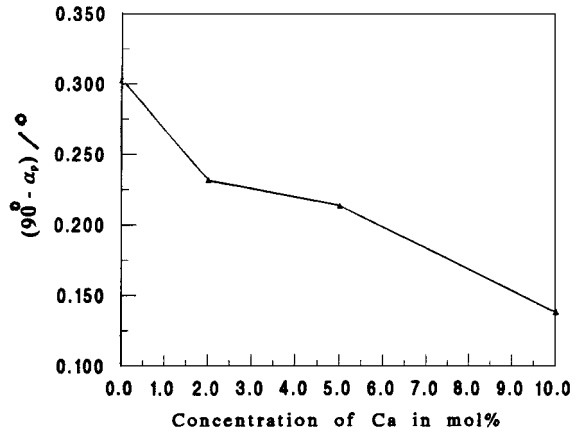

Figure 6 Rhombohedral lattice strain ($90^\circ - \alpha_p$) as a function of Ca^{2+} content for $Pb_{1-y}Ca_y(Zr_{0.8}Ti_{0.2})O_3$ system.

3.2. Density measurements

Fig. 7 shows the variation, with Ca^{2+} concentration, of the ratios of measured density to X-ray density, the value of the measured densities being the average values of at least three different samples of the same composition. As can be seen in Fig. 7, the undoped sample in this series has the lowest density compared to that of 2 and 5 mol% Ca^{2-} doped samples, where the measured density is close to theoretical density. However, the density is lower again in case of the 10 mol% Ca^{2+} doped composition.

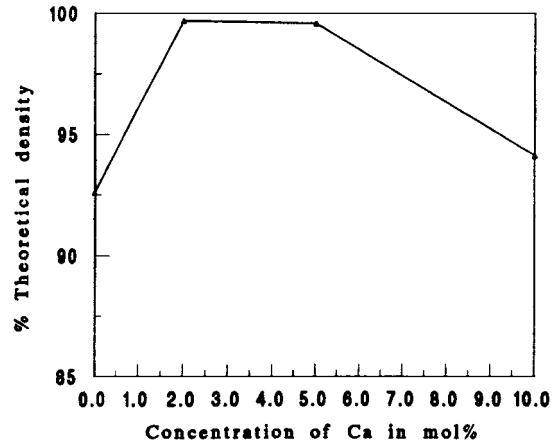

Figure 7 Density (% of theoretical density) as a function of Ca^{2+} content for $Pb_{1-y}Ca_y(Zr_{0.8}Ti_{0.2})O_3$ system.

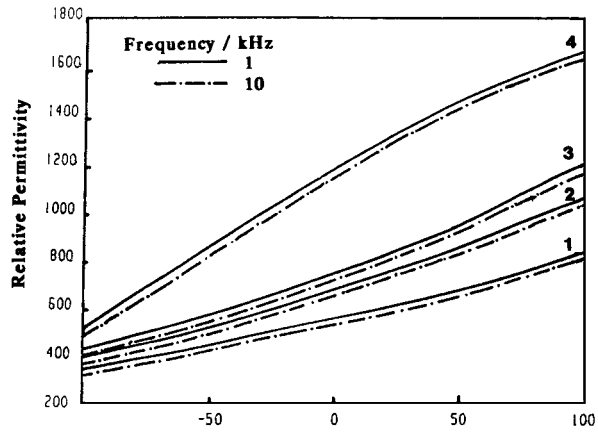

Figure 8 Relative permittivity as a function of temperature for $Pb_{1-y}Ca_y(Zr_{0.8}Ti_{0.2})O_3$ system measured at two different frequencies: (1) $y=0$, (2) $y=0.02$, (3) $y=0.05$ and (4) $y=0.1$, all samples are hot-pressed at 1200°C for 1 h.

3.3. Dielectric properties

3.3.1. Low temperature measurements

Fig. 8 demonstrates the variation of relative permittivity with temperature for this series of compositions between −100 and 100°C, using the low-temperature measurement rig at 1 and 10 kHz. Samples doped with Ca^{2+} generally have higher relative permittivities in this temperature range compared to the undoped compositions of this series, i.e. PZT(0.8). The sample doped with 10 mol% shows the highest relative permittivity throughout the whole range of low temperature measurement.

3.3.2. High temperature measurements

Dielectric measurements were carried out between room temperature and 400°C at four different frequencies, 1 kHz, 10 kHz, 100 kHz and 1 MHz. Fig. 9 presents the variation of relative permittivity (ε_r') with temperature at 10 kHz for this compositional series. No relaxor behaviour, i.e. frequency shift in the magnitude of $T'\varepsilon_{r,max}$, the temperature at which ε_r' reaches a maximum, was observed for any of the samples, when measured at four different frequencies. This can be seen in Fig. 10, which gives the variation of relative permittivity ε_r' with temperature for one of the compositions of

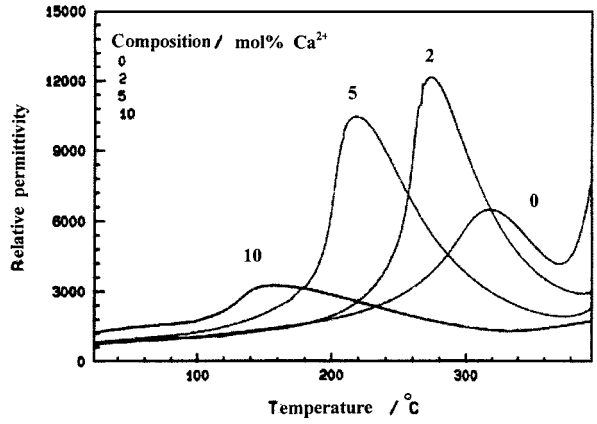

Figure 9 Relative permittivity as a function of temperature for $Pb_{1-y}Ca_y(Zr_{0.8}Ti_{0.2})O_3$ system measured at 10 kHz; all samples are hot-pressed at 1200°C for 1 hr.

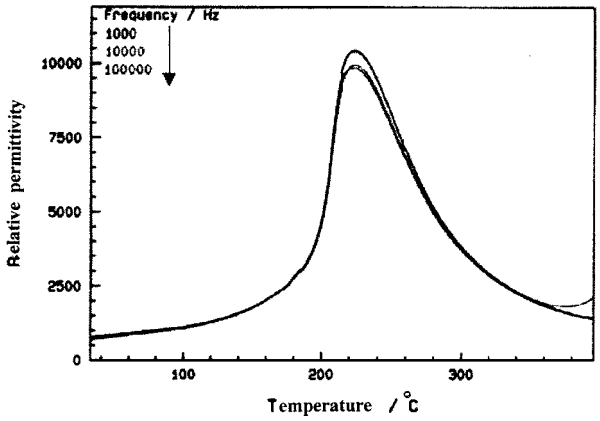

Figure 10 Relative permittivity as a function of temperature at various frequencies for 5 mol% Ca^{2+}-doped PZT(0.8), hot-pressed at 1200°C for 1 hr.

this series (PZT(0.8) doped with 5 mol% Ca^{2+}) at three different frequencies. The rapid rise observed in the 1 kHz and 10 kHz curves at temperatures much higher than Curie temperature (as can be seen in Figs 9 and 10) is believed to be due to a conduction process taking place in these samples at these temperatures. For the composition PZT(0.8) doped with 10 mol% Ca^{2+}, the variation of ε_r' with T, as shown separately in Fig. 11, is diffuse. Furthermore, the ε_r'-T curve corresponding to the undoped sample PZT(0.8), which had the lowest density compared to that of 2 and 5 mol% Ca^{2+} doped samples, is also quite broad and unexpectedly low (Fig. 9). Therefore an attempt was made to obtain another sample of this composition, with larger grain size and higher density. Hot-pressing was used at a higher temperature i.e. 1300°C for 2 hrs. Fig. 12 shows the result obtained for the variation of ε_r'-T curve at different frequencies for undoped sample hot-pressed at 1300°C for 2 hrs. As can be seen from this figure, a much sharper and higher value of $\varepsilon'_{r,max.}$ was obtained for this sample.

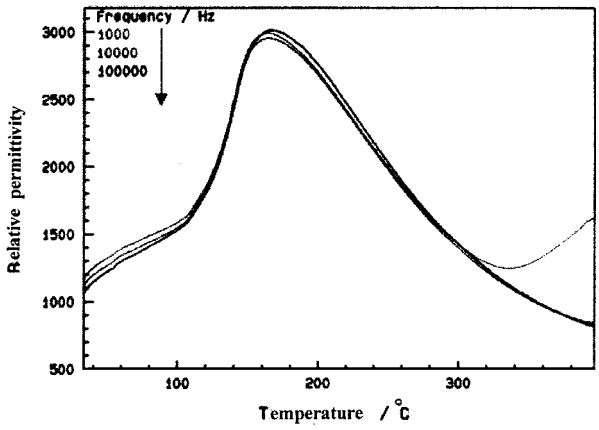

Figure 11 Relative permittivity as a function of temperature at various frequencies for 10 mol% Ca^{2+}-doped PZT(0.8), hot-pressed at 1200°C for 1 hr.

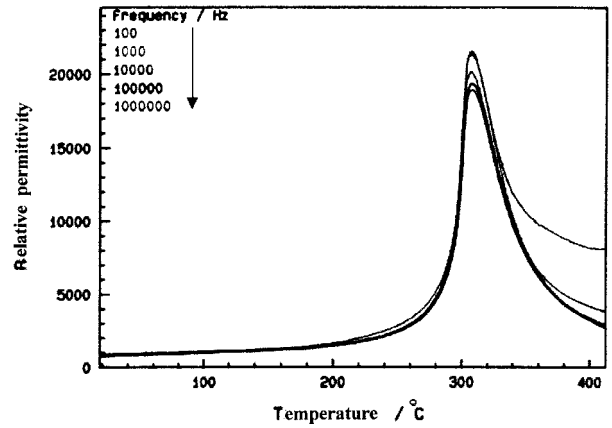

Figure 12 Relative permittivity as a function of temperature at various frequencies for undoped PZT(0.8), hot-pressed at 1300°C for 2 hrs.

However, this wasn't the case for the composition PZT(0.8) doped with 10 mol% Ca^{2+} when hot-pressed at 1300°C for 2 hrs. A higher density (98%) and larger grain sizes (in the range between 2–5 μm) were obtained compared to the samples hot-pressed at 1200°C for 1 hr (Fig. 13). Fig. 14 shows the results obtained for the variation of ε_r'-T curve at different frequencies for PZT(0.8) doped with 10 mol% Ca^{2+} hot-pressed at 1300°C for 2 hrs. As can be seen in this

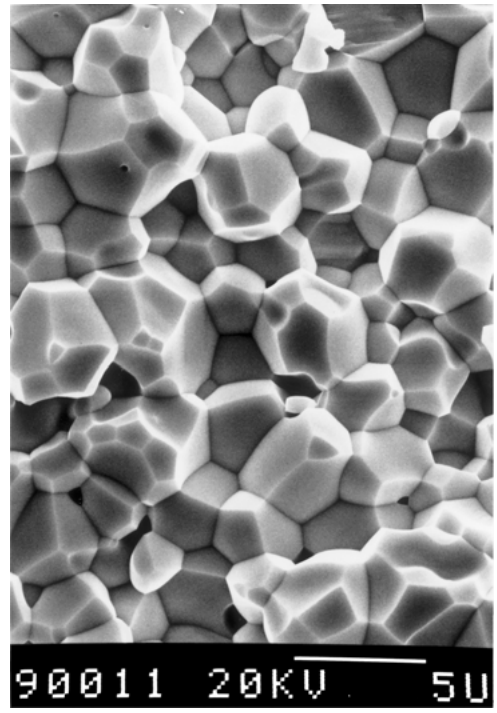

Figure 13 SEM micrograph of $Pb(Zr_{0.8}Ti_{0.2})O_3$ doped with 10 mol% Ca^{2+}; hot-pressed at 1300°C for 1 h.

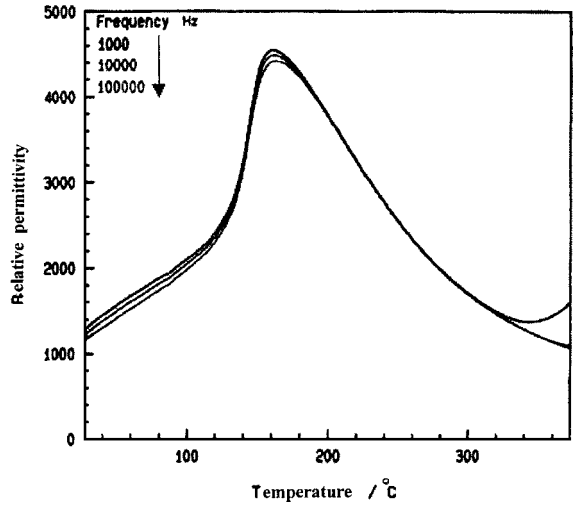

Figure 14 Relative permittivity as a function of temperature at different frequencies for 10 mol% Ca^{2+}-doped PZT(0.8), hot-pressed at 1300°C for 2 hrs.

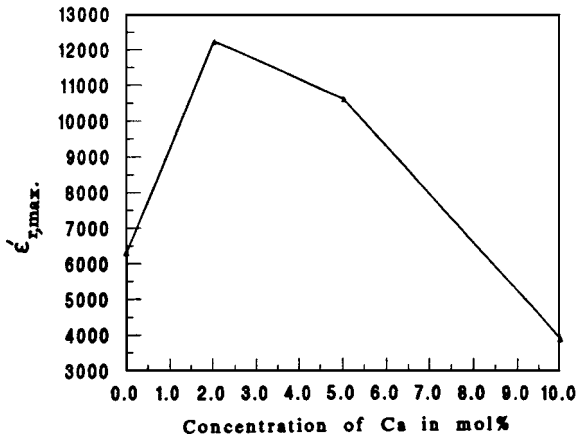

Figure 15 Maximum relative permittivity, $\varepsilon'_{r,max}$ as a function of Ca^{2+} content for $Pb_{1-y}Ca_y(Zr_{0.8}Ti_{0.2})O_3$ system, all samples are hot-pressed at 1200°C for 1 hr.

curve, the diffuseness of the ε'_r-T curve for PZT(0.8) doped with 10 mol% Ca^{2+} is maintained, with a slight increase in the magnitude of $\varepsilon'_{r,max}$. This suggests that the diffuseness in ε'_r-T for the case of PZT(0.8) doped with 10 mol% Ca^{2+} is not due to microstructural factors. Since the use of high temperatures could jeopardize the careful attention to minimisation of the Pb loss, these sintering conditions i.e. 1300°C for 2 hrs, were not adopted for all of the samples in this work. The variation of the maximum relative permittivity $\varepsilon'_{r,max}$ at 10 kHz with Ca^{2+} concentration is shown in Fig. 15. The samples doped with 2 and 5 mol% Ca^{2+} have a higher maximum relative permittivity than that of 10 mol% doped sample, which had the lowest relative permittivity amongst this series of compositions. Furthermore, for this composition the curve of the variation of ε'_r with T is very diffuse (Fig. 11), making it rather difficult to assign a precise value for the Curie temperature. The variation of Curie temperature with Ca^{2+} concentration is given in Fig. 16. The magnitude of Curie temperature on this graph is taken as temperature where the maximum relative permittivity $\varepsilon'_{r,max}$ occurs. It is seen that the Curie temperature decreases linearly with increase of Ca^{2+} concentration.

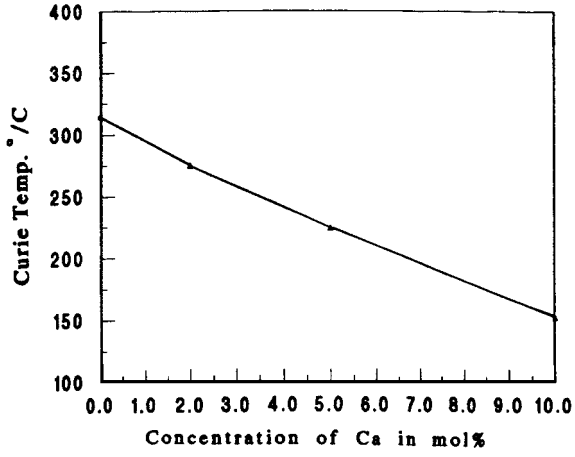

Figure 16 Curie temperature as a function of Ca^{2+} content for $Pb_{1-y}Ca_y(Zr_{0.8}Ti_{0.2})O_3$ system, all samples are hot-pressed at 1200°C for 1 hr.

3.4. Polarization measurements

Fig. 17 shows a multiplot of the variation of polarization versus applied electric field at room temperature, the so called "Sawyer-Tower" loop, for this series of compositions. As can be understood from this multiplot, adding up to 10 mol% Ca^{2+} to PZT(0.8) gives rise to a remarkable reduction of polarization. Fig. 18 gives the variation of spontaneous polarization (P_s) with Ca^{2+} concentration at room temperature. The value of spontaneous polarization in this graph is obtained by extrapolating the tips of the Sawyer-Tower loop where the polarization reaches to its maximum value. The intercept of this line on the polarization axis is taken as P_s. As Fig. 18 implies, the magnitude of P_s drops remarkably

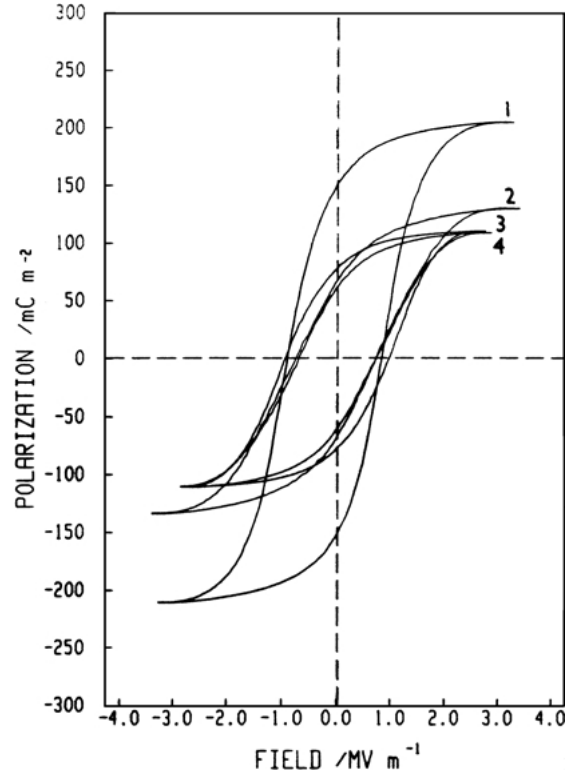

Figure 17 Polarization as a function of electric field for $Pb_{1-y}Ca_y(Zr_{0.8}Ti_{0.2})O_3$ system: $y = 0$(1), $y = 0.02$ (2), $y = 0.05$ (3) and $y = 0.1$ (4), all samples are hot-pressed at 1200°C for 1 hr.

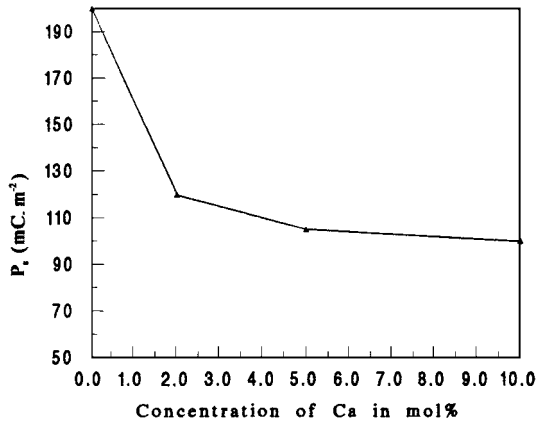

Figure 18 Saturation polarization, P_s, as a function of Ca^{2+} content for $Pb_{1-y}Ca_y(Zr_{0.8}Ti_{0.2})O_3$ system, all samples are hot-pressed at 1200°C for 1 hr.

on doping PZT(0.8) with 2 mol% Ca^{2+}. However, the rate of decrease slows down for Ca^{2+} concentrations above 2 mol%. Doping PZT(0.8) with 2 and 5 mol% Ca^{2+} reduces the coercive field. However, in the case of 10 mol% Ca^{2+} concentration the coercieve field increases again and becomes even higher than that of undoped PZT(0.8).

4. Discussion

4.1. Crystalline structure

XRD results revealled no structural change for PZT(0.8); (Zr/Ti = 80/20) when doped with 2, 5 and 10 mol% Ca^{2+}, with a linear decrease of lattice parameter (a_α) with Ca^{2+} concentration (Fig. 4). Both RH lattice distortions ($90^\circ - \alpha_R$) and lattice parameters (a_p) decreased for the compositions of rhombohedral structures when Ca^{2+} was substituted for Pb^{2+}. The magnitude of the decrement of these was raised by increasing the content of Ca^{2+}. This is possibly because Pb^{2+} in RH PZT froms [17] PbO_3 dipoles which along with TiO_3 dipoles yield a large spontaneous polarization and also a strong lattice distortion, i.e. expansion along the polarization direction and contraction in perpendicular directions. However, when Ca^{2+} is substituted for Pb^{2+}, since it does not form similar directional bonding, it is likely that the lattice distortion observed in the case of undoped PZT compositions, decreases. As mentioned before, substituting Ba^{2+} for Pb^{2+} in PZT, is seen to decrease the RH lattice distortion as well. The magnitude of the decline also increases as the Ba^{2+} content increases. A similiar argument to that used for calcium-doped PZT compositions can perhaps be extended to Ba^{2+} substituted compounds as well. The high electronegativity of the Ba–O bond (2.6) compared to that of the Pb–O bond (1.7) yields an ionic component of 82% compared to 49% for Pb–O [18]. Thus barium does not form directional bonding similar to lead, with consequent strong lattice distortion.

4.2. Bulk density

PZ-rich PZT compounds normally show poor sinterability due to the low reactivity of ZrO_2 powder, especially at low sintering temperatures. Adding Ca^{2+} up to 5 mol%, however, to this series of compositions increased the density appreciably. This might be due to the fact that calcium has acted as a liquid phase sintering aid during the sintering (hot-pressing) process, thereby improving the density, though without a remarkable effect on grain size. The degree of improvement of ceramic density due to introduction of a liquid phase sintering aid is, however, normally limited up to a critical level of liquid phase content [19], above which it has an adverse effect. This is likely to be the reason why adding 10 mol% Ca^{2+} to PZT(0.8) has decreased the density again. Of course, the lower atomic weight of calcium compared to lead should also be considered in this respect as well.

4.3. Crystal–chemical interpretation of the observed ferroelectric response

In perovskites, the dipolar units correspond physically to unit cells of the structre, which are coupled both electronically and vibrationally. Therefore a significant elastic component to the dipolar coupling is expected, in contrast to the case of a pure dielectric medium where the forces coupling dipoles are entirely electrostatic in origin. The stabilization of a spontaneously polarized ferroelectric phase requires permanent dipoles, as well as coupling between them. In the absence of this coupling, a system of isolated dipoles dominates. Fig. 19a shows the coordination of a central BO_6 octahedron by the 26 BO_6 octahedra in adjacent unit cells. Of these 26 octahedra, six are related to the central octahedron by ⟨100⟩ translation vectors. Fig. 19b, 12 are related by ⟨110⟩ vectors (Fig. 19c), and eight by ⟨111⟩ vectors (Fig. 19d).

It is only the ⟨100⟩-related octahedra which share corners with the central octahedron, so direct BO_6-BO_6 coupling is possible only in ⟨100⟩ directions. There is also the possibility of indirect BO_6-BO_6 coupling, which is transmitted via the lead ions. Direct ⟨100⟩-coupling in PZ-rich PZT between Ti^{4+} and Zr^{4+} octahedra is likely to be very weak. Zr^{4+}, due to its large size compared to that of titanium, forms a very tightly coordinated polyhedron, thereby making it ferroelectrically inactive by occupying a centred position inside its polyhedral cage. The distribution of Zr^{4+} and Ti^{4+} ions over B-sites in pure PZT can be considered as completely random. It can be also appreciated that the coupling of given ferroelectrically active TiO_6 octahedron to the ferroelectric network depends on the ratio of Zr^{4+} and Ti^{4+} ions occupying ⟨110⟩-related B-sites. In the case of compositions with a high concentration of Zr^{4+}, therefore, the contribution of direct ⟨100⟩-coupling will be negligible, particularly due to the higher probabilities of occurrence of Zr^{4+}-Zr^{4+} or Zr^{4+}-Ti^{4+} linkages, rather than Ti^{4+}-Ti^{4+}. In the case of indirect ⟨110⟩-oriented coupling, three kinds of ⟨110⟩-linkage can be assumed: Zr-Pb-Zr, Ti-Pb-Zr, and Ti-Pb-Ti. The first linkage can be considered as an inactive linkage and Ti-Pb-Ti as the strongest one, which couples a TiO_6 octahedra to the other active TiO_6 octahedra: the presence of Zr^{4+} in a ⟨110⟩-related B-site weakens the coupling of central

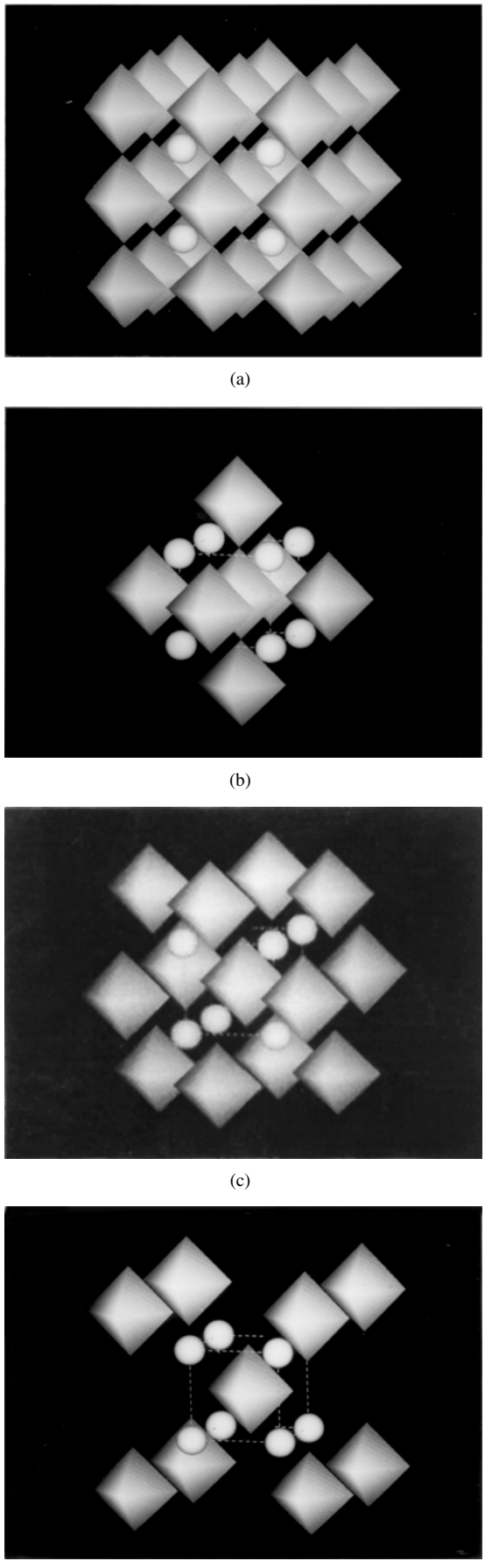

Figure 19 The perovskite structure, ABO_3, with A ions represented as spheres, and BO_6 octahedra highlighted. Coordination is shown of a central BO_6 octahedron by: (a) 26 translationally related BO_6 octahedra, in adjacent unit cells, (b) six ⟨100⟩-related BO_6 octahedra, (c) 12 ⟨110⟩-related BO_6 octahedra, and (d) eight ⟨111⟩-related BO_6 octahedra.

TiO_6 octahedron to the ferroelectric network. The indirect [110] link proceeds via two lead ions, with elementary linkages given by 1/2 [111] and 1/2 $[\bar{1}\bar{1}\bar{1}]$. The importance of indirect ⟨110⟩- or $\langle\bar{1}\bar{1}\bar{1}\rangle$ coupling in PZT suggests that the presence of lead ion is a requirement for ferroelectric properties. In case of substitution of Ca^{2+} for Pb^{2+}, these three ⟨110⟩ oriented coupling will be overall much weaker compared to the cases of undoped composition, with an overall effect of weakening of ferroelectric response for these compounds. The long-range coupling of BO_6 octahedra is a necessary requisite for a perovskite structure to show ferroelectricity [20]. However, this issue is likely to be influenced by BO_6 octahedra as well as the influence of the A-site cation on O^{2-} ion displacement. For the compositions studied here in this work, a continuous compositional variation throughout the material is assumed. In perovskites, the A-ion is ideally coordinated with twelve oxygen ions, occupying the cuboctahedral site. Since Ca^{2+} does not form a directional ionic bond with oxygen, it can be assumed that it is situated at the centre of this oxygen anion cage. The directionality associated with the covalent Pb─O bond means that lead prefers 3-, or 4-fold coordinated structures, which can be achieved by displacement towards triangular or square faces of the cuboctahedral cage respectively. However a 3-fold coordinated structure may be favoured, on chemical grounds [21], because the formation of 4 sp^3 hybridised atomic orbitals becomes possible, with the lone pair on the lead ion occupying the orbital pointing away from the triangular face. While one orbital can be occupied by the lone-pair of electrons, the others accept electrons from the coordinating oxygen. The 3 oxygens which coordinate the lead also form a face of a BO_6 octahedra. This will give rise to the coupling of lead and the Zr/Ti cations in the ⟨111⟩ directions, making the long-range ferroelectric coupling of $(Zr/Ti)O_6$ octahedra possible, and ensuring the occurrence of ferroelectricity in PZT.

In case of PZ-rich PZT compounds, the oxygen octahedra are tilted about [111], which gives rise to a doubling of the unit cell. The tilting causes the B cation-anion bond in one octahedron to rotate in an opposite direction to that in a neighboring octahedron, thus giving rise to a doubling of the repeat distance. If one attempts to maintain the B cation-anion bond distance one must expect the B cation-B cation distance to become shorter and hence reduce the axial length. Rotation of oxygen octahedra decreases the volume available to the A cation. Megaw and Darlington [22] have suggested that the angle of rotation of an oxygen octahedron (tilt angle) depends primarily on packing round the A cation and hence on the size of A. Therefore, it can be anticipated that substitution of Ca^{2+} for Pb^{2+} in PZT, for example, is likely to increase tilt angle, due to its smaller ionic size compared to Pb^{2+}. N. W. Thomas and Ali Beitollahi [23], for the first time based on a systematic work, have shown that for various ferroelectric perovskites of (RH) structures but of different space groups a unique correlation between V_A/V_B ratio and tilt angle exists. The unique correlation observed by them suggests that for a specified value of tilt angle both A site and B site polyhedral volumes

adjust themselves to satisfy the magnitude of the tilt angle. This implies that the magnitude of the tilt can possibly be tailored by varying V_A/V_B ratio through the appropriate choice of ions of different sizes. This provides a powerful tool for predicting the magnitude of tilt. Although this unique variation is observed for different compositions of (RH) structure of various space groups, there is no reason why one shouldn't assume that such a trend is likely to happen for a fixed composition (such as PZT) with RH structure and varying A/B-site cation concentrations. In fact, it is interesting to note that Corker *et al*. [24] have recently verified experimentally for RH PZT compounds of varying Zr/Ti ratio that the octahedral tilt angle decreases with the increase of TiO_2 content, confirming the prediction made by N. W. Thomas and A. Beitollahi [23]. Clarke and Glazer [25] have also given the correlation between the Gibbs free energy and octahedral tilt angle and strain. The importance of the octahedral tilt angle in calculating saturation polarization is also raised by Haun *et al*. [26]. In their thermodynamic phenomenological approach, they have introduced a tilt related term in their calculation of saturation polarization, emphasizing the importance of the tilt in this respect. For the samples studied in this work, neutron diffraction measurements are currently under way to investigate the effect of the substitution of Ca^{2-} on the magnitudes of the octahedral tilt angle and strain.

4.4. Low-field relative permittivity

For a normal ferroelectric the maximum relative permittivity appears on heating through the ferroelectric-paraelectric transition. In case of strong coupling, the ferroelectric activity of $(Zr/Ti)O_6$ octahedra, i.e., the stabilisation of Zr^{4+}/Ti^{4+} ions at off-centre sites, is high. This is likely to give rise to a high relative permittivity at the transition temperature. A compositional system similar to the system studied in this work is anticipated to have a distribution of coupling strength, due to a random distribution of Ca^{2+} in A(Pb)-sites. In the case of a narrow distribution of coupling strengths the proportion of transforming regions from ferro- to paraelectric phase at a given temperature is high. Therefore, the highest relative permittivity for these compositions can be expected for those of strongest coupling and minimum compositional fluctuations. i.e., towards the PZT-end of the solid solution. Substitution of calcium is, however, likely to reduce the coupling strength and increases compositional variation on the A-sites, therefore causing reductions in $\varepsilon'_{r,max.}$. This is in agreement with the results obtained for PZT(0.8) doped with 10 mol% Ca^{2+}, where the magnitude of $\varepsilon'_{r,max.}$ is reduced appreciably compared to the undoped composition, which also had the lowest bulk density amongst all the samples of this series. It worth noting that normally in ferroelectrics the relative permittivity increases with increasing density, to a certain extent.

Substituting Pb^{2+} with Ca^{2+} or Sr^{2+} in PZT [27] causes an increase in the room temperature relative permittivity. A higher relative permittivity is also observed for the low-temperature measurement range (Fig. 8) for Ca^{2+}-doped PZT(0.8) compositional series studied in this work. This increase can be explained in terms of a simple molecular argument. At low temperatures close to $-100°C$ for these compositional series the effect of increasing temperature is to provide the thermal expansion required to enlarge the octahedral interstice occupied by Zr/Ti, providing a greater freedom of movement, and therefore, a higher electric susceptibility. No relaxor behaviour, which is a frequency shift in $T\varepsilon'_{r,max.}$ was observed for any of the compositions of this solid solution system. Butcher and Thomas [28], using the coupling model, have proposed a tentative explanation for the dielecric mechanism in PMN. They have suggested that the distribution in coupling strengths due to B-site effects in PMN produces a distribution in relaxation times, τ; strongly coupled regions having short τ and weakly coupled regions having long τ. All regions respond at low frequencies, but increasing frequency causes progressive relaxation of weakly coupled regions. At high frequencies, only strongly coupled regions with high local transition temperatures and short τ respond. Therefore, the influence of increasing frequency will have two effects: (i) $\varepsilon'_{r,max.}$ is reduced because fewer coupled regions participate in the dielectric response; and (ii), the Curie temperature shifts towards higher temperature. However, a diffuse and broad variation of the ε'_r-T response was observed for PZT(0.8) doped with 10 mol% Ca^{2+}, which has been observed to be a single phase rhombohedral structure at room temperature. Diffuse phase transitions (DPT) in ferroelectric perovskites were originally studied by Smolenskii and Agranovskaya [29]. They were the first to propose that the diffuse phase transition (DPT) observed in $PbMgNbO_3$ (PMN), is due to the compositional fluctuations in this compound. They have suggested that, in this compound, regions were established which were rich or depleted in Nb^{5+} relative to the stoichiometric composition. For niobium-deficient regions, due to weak coupling disrupted by low thermal energy, a low local transition temperature is likely to occur. However, the strong coupling of Nb-rich regions leads to high local transition temperatures, explaining the DPT in terms of the distribution in coupling strengths due to B-site disorder. The Curie temperature in this case can be interpreted as the transition temperature of the 'average' composition, when most coupled regions transform, giving rise to a maximum in dielectric susceptibility.

Extending Smolenskii's ideas to the PZT(0.8) composition doped with 10 mol% Ca^{2+}, it can be expected that, due to a random A-site occupancy of Ca^{2+} in this composition, fluctuations in composition of both A- and B-sites increase the distribution in coupling strengths. Therefore it can be anticipated that the material is composed of different regions each of different Curie temperatures. This distribution of coupling strengths gives rise to a variation of Curie temperature of the compositionally different regions. For regions with higher lead concentrations, the existence of higher transition temperatures is expected. However, for the regions of lower Pb^{2+} i.e. of higher calcium concentration, due to the weakening of coupling strength, a lower

transition temperature is anticipated. The difference between the transition temperature of these regions and that of the average composition will be high, resulting in increased phase transition diffuseness. In contrast, for a ferroelectric compound such as $BaTiO_3$ which has an identical ionic environment, a unique strength of the coupling between dipoles can be anticipated. Random compositional fluctuation of Ca^{2+} and Pb^{2+} substituted A-sites, according to this model, is likely to be responsible for the diffuse phase transitions observed in the case of the 10 mol% Ca^{2+}-doped PZT(0.8) composition studied here in this work. The greater the extent of compositional variation, by incorporating higher Ca^{2+} concentrations in this compound, the greater the distribution in coupling strengths in these compounds would be, with a greater degree of diffuseness in the phase transition. A diffuse and broad variation of the ε'_r-T curve, is also observed for Ba^{2+}-doped and Sr^{2+}-doped PZT [13], with increasing Ba^{2+} and Sr^{2+} concentration.

4.5. Saturation polarisation

Doping PZT(0.8) with Ca^{2+} decreased saturation polarisation. This is in agreement with the coupling model presented here in this work, which proposes that Ca^{2+} interrupts long-range ferroelectric coupling between B (Zr/Ti) octahedra. The reduction of coercive field in case of 2 and 5 mol% Ca^{2+}-doped PZT(0.8) could possibly be due to the increase in density of these two samples compared to that of undoped PZT(0.8) sample. For PZT(0.8) doped with 10 mol% Ca^{2+} since the density decreases again, the coercive field increases as well.

5. Conclusions

The below mentioned conclusions are obtained regarding the study carried out in this work:

1. Ca^{2+} interrupts the long–range ferroelectric coupling between Zr/Ti octahedra which would have occurred when only Pb occupied the A-site with a consequent reduction of the curie temperature.

2. The diffuse phase transition observed in the case of 10 mol% Ca^{2+}-doped PZT(0.8) is believed to be due to the distribution in coupling strengths created from a random compositional fluctuations of Ca^{2+} and Pb^{2+} ions on A-sites.

3. No structural changes were observed for the whole range of the samples studied in this work by Ca^{2+} incorporation.

4. A linear decrease of RH lattice constant a_p is seen with increasing the Ca^{2+} concentration with a subsequent decrease of lattice strain expressed by $(90 - \alpha_p)$.

5. A sharp decline is observed in the magnitudes of saturation polarisation (P_s) of the samples doped with 2 mol% Ca^{2+}. However, the rate of decrease slows down for Ca^{2+} concentrations above this level.

Acknowledgements

Acknowledgement is made of N. W. Thomas for his kind help during the work. Acknowledgement is also due to Iran Ministry of Science, Research and Technology (MSRT) for the finance of the work.

References

1. B. JAFFE, W. R. COOK and H. JAFFE, "Piezoelectric Ceramics" (Academic Press, London, 1971).
2. R. W. WHATMORE, *Rep. Prog. Phys.* **49** (1986) 1335.
3. B. NOHEDA, D. E. COX, G. SHIRANE, J. A. GONZALO, S.-E. PARK and L. E. CROSS, *Appl. Phys. Lett.* **74** (1999) 2059.
4. B. NOHEDA, J. A. GONZALO, L. E. CROSS, R. GUO, S.-E. PARK, C. MOURE, D. E. COX and G. SHIRANE, *Phys. Rev.* B **61** (2000) 8687.
5. A. G. SOUZA FILHO, K. C. V. LIMA, A. P. AYALA, I. GUEDES, P. T. C. FREIRE, J. MENDES FILHO, E. B. ARAUJO and J. A. EIRAS, *Phys. Rev.* B **61** (2000) 14283.
6. J. HANDEREK, J. KWAPULINSKI, Z. UJIMA and K. ROLEDER, *Ferroelectrics* **81** (1988) 253.
7. J. HANDEREK, J. KWAPULINSKI, M. PAWELCZYK and Z. UJIMA, *Phase Transitions* **6** (1985) 35.
8. Z. UJIMA, J. HANDEREK, M. PAWELCZYK, H. HASSAN, E. G. KUGEL and C. CARABATOS-NEDELEC *J. Phys.: Condens. Matter* **6** (1994) 6843.
9. Y. I. CHANG, *Appl. Phys.* A **29** (1982) 237.
10. C. MICHEL, J. M. MOREAU, G. D. ACHENBACH, R. GERSON and W. J. JAMES, *Commun. Solid St. Phys.* **7** (1969) 865.
11. A. M. GLAZER, *Acta Crystallogr.* B **28** (1972) 3384.
12. *Idem.*, *ibid.* A **31** (1975) 756.
13. T. IKEDA, *J. Phys. Soc. Jap.* **14** (1959) 168.
14. *Idem.*, *ibid.* **14**(10) (1959) 1286.
15. G. SHIRANE and S. HOSHINO, *Acta. Cryst.* **7** (1954) 203.
16. A. BEITOLLAHI, Ph.D. Thesis, 1992, School of Materials, University of Leeds, UK.
17. H. THOMMANN, *Ferroelectrics* **73** (1987) 183.
18. L. PAULING, "The Nature of the Chemical Bond," 3rd ed. (Cornell University Press, New York).
19. W. D. KINGERY, "Introduction to Ceramics" (J. Wiley & Sons, New York).
20. H. D. MEGAW, "Ferroelectricity in Crystals" (Methuen, 1957).
21. W. HEYWANG and H. THOMMAN, *Ann. Rev. Mater. Sci.* **14** (1984) 27.
22. H. D. MEGAW and C. N. W. DARLINGTON, *Acta Cryst.* A **31** (1975) 161.
23. N. W. THOMAS and A. BEITOLLAHI, *ibid.* **B50** (1994) 549.
24. D. L. CORKER, A. M. GLAZER, R. W. WHATMORE, A. STALLARD and F. FAUTH, *J. Phys.: Condens. Matter* **10** (1998) 6251.
25. R. CLARKE and A. M. GLAZER, *Ferroelectrics* **12** (1976) 207.
26. M. J. HAUN, E. FURMAN, S. J. JANG and L. E. CROSS, *Ferroelectrics* **99** (1989) 13.
27. F. KULCSAR, *J. Amer. Ceram. Soc.* **42**(1) (1959) 49.
28. S. J. BUTCHER and N. W. THOMAS, *J. Phys. Chem. Solid* **52** (1991) 595.
29. G. A. SMOLENSKII and A. I. AGRANOVSKAYA, *Soviet Phys. Solid State* **1**(14) (1959) 29.

Received 9 April
and accepted 25 November 2002